Precipitation Characteristics of HPVDC AlSi10Mg0.3Mn Alloy under Different Temper Conditions

Z. Chen, E.M. Elgallad*, K. Liu, X.-G. Chen
Department of Applied Science, University of Quebec at Chicoutimi,
Saguenay (QC), Canada G7H 2B1

Abstract

This work studied the precipitation characteristics of AlSi10Mg0.3Mn alloy produced by high-pressure vacuum die-casting (HPVDC) in T5 and T6 conditions using transmission electron microscopy, differential scanning calorimetry and both electrical conductivity and microhardness measurements. Two different T6 tempers were used, involving partial solutionizing at 460 °C for 1 h and full solutionizing at 500 °C for 1 h, and were designated as T6P and T6F, respectively. The aging treatment was conducted at 185 °C for 4 h in all temper conditions. The results showed that conducting solution treatments resulted in the formation of α-Al(MnFe)Si dispersoids. In addition, Mg-Si rich precipitates formed and remained undissolved after partial solutionizing. The highest supersaturation of the α-Al was achieved in the as-fabricated (F) condition by the HPVDC process. The supersaturation degree decreased in both partial and full solutionizing conditions. TEM observations revealed different precipitation characteristics for T5, T6P and T6F tempers. *β''* precipitates just started to form in the T5 condition, whereas both *β''* and *β'* precipitates completed their precipitation to different extents in the T6P and T6F conditions, resulting in different strengthening effects. The T6F temper yielded the highest microhardness followed by the T5 and T6P tempers.

Keywords: Al-Mg-Si cast alloys; high pressure vacuum die casting; heat treatments, microstructure characterization.

*Corresponding author Tel.: +1 418 545 5011 # 2558; Fax: +1 418 545 5012.
E-mail address: eelgalla@uqac.ca (E.M. Elgallad)

1. Introduction

In recent years, aluminum castings are being used to an ever-increasing extent for structural components in both the automotive and aerospace industries to reduce the weight of vehicles and consequently the greenhouse gas emissions. High-pressure die-casting is a sophisticated process used for the mass production of aluminum castings because it is suitable to produce arbitrary complicated shapes with a high production rate. High-pressure vacuum die-casting (HPVDC) was reported to reduce significantly the porosity in the cast parts, which is caused by the entrapment of air in the molten metal during the casting process [1]. Therefore, HPVDC technique can be adopted to manufacture thin-walled parts with complicated geometry.

AlSi10Mg0.3Mn alloy (Aural-2) was developed based on the binary Al-Si system. The Si level is selected close to the eutectic composition to enhance the fluidity and the die-filling capability required to produce thin-walled complex shapes with large surface areas. Manganese is added to prevent die soldering of die castings by inhibiting the formation of the needle-like β-Al_5FeSi intermetallic phase and promoting the formation of the Chinese script α-$Al_{15}(Fe,Mn)_3Si_2$ phase that facilitates demolding in comparison with the needle-like phase [2,3]. The precipitation hardening of this alloy occurs according to the general precipitation sequence of Al-Si-Mg alloys as follows [4-6]: supersaturated solid solution (SSS) → Mg-Si clusters/co-clusters → *GPI* → *β''* (*GPII*) → *β'* → *β*-Mg_2Si, where *GPI* refers to Guinier-Preston (GP) zones and *β''* and *β'* are the precursors of the equilibrium *β*-Mg_2Si phase.

Generally, high-pressure die-cast aluminum alloys are not supposedly heat-treated to T6 temper because the traditional solution heat treatments involved enlarge the pores that arise from the trapping of gas during the die-casting process, resulting in the undesirable surface blistering [7]. Therefore, these alloys are usually heat-treated to T5 tempers that yield high strengths at the expense of ductility. However, the need to improve the ductility of high-pressure die-cast aluminum components may necessitate solutionizing these components prior to the artificial aging while avoiding the undesirable surface blistering. This could be achieved by adopting T6 tempers involving low-temperature solution heat treatments with short soaking times.

The precipitation characteristics of high-pressure die-cast Al-Si-Mg alloys, which control their mechanical properties, have not yet been widely studied in the T6 condition with reference to the T5 condition, particularly for the alloys produced by HPVDC. The present work is, therefore, undertaken to study the precipitation characteristics of a HPVDC AlSi10Mg0.3Mn alloy in T5 and two different T6 conditions. The two T6 conditions involved two short solution heat treatments, namely partial and full

solution heat treatments. The precipitation characteristics were studied using transmission electron microscopy (TEM), differential scanning calorimetry (DSC) and both electrical conductivity (EC) and microhardness measurements.

2. Experimental Procedures

The AlSi10Mg0.3Mn alloy used in this study was supplied in the form of 220 × 65 × 3 mm thin plates produced by HPVDC with a chemical composition listed in Table 1. The as-cast alloy was then heat-treated to T5 temper and two different T6 tempers as explained in Table 2. All heat treatments were conducted in a programmable air circulating electric furnace.

Heat-treated samples were mounted, ground and polished according to the standard metallographic preparation for the microstructural examination with a Nikon Eclipse ME600 optical microscope. The precipitates formed under different heat treatment conditions were observed using a JEOL JEM-2100 transmission electron microscope (TEM) operated at 200kV in conjunction with an energy-dispersive spectroscopy (EDS). The TEM samples were electropolished to perforation for approximately 1 min at –20 ºC and 12 V using a twinjet electropolisher. The electrolyte was a mixture of nitric acid and methanol with a volume ratio of 1:2. The number density of the precipitates, *D*, was calculated from the following equation [8,9]:

$$D = \frac{3N_{\parallel}}{A(t + \langle l \rangle)} \tag{1}$$

where $N_{\parallel}$ is the number of precipitate cross-sections in the imaged area, A, and $\langle l \rangle$ is the average needle length. The factor 3 accounts for the three equivalent directions of $\langle 100 \rangle_{\mathrm{Al}}$ in which the needles grow, assuming an isotropic distribution. The TEM foil thickness, *t*, was measured according to the diffraction fringes [10,11]. Both $N_{\parallel}$ and $\langle l \rangle$ were determined from TEM images using the image analyzer Clemex PE 4.0.

DSC analysis was carried out with a Mettler Toledo computerized differential scanning calorimeter under a protective atmosphere of pure argon at a follow rate of 30 mL/min. The mass of the DSC sample was approximately 20 mg. The DSC heating scans were recorded in the temperature range of 50 °C to 550 °C at a heating rate of 10 °C/min. Electrical conductivity measurements were made on polished samples at room temperature with a Sigmascope SMP10 eddy current electrical conductivity meter based on the percentage of international annealed copper standard (%IACS). Eight measurements

were taken and averaged per condition. A Vickers microhardness test was conducted under an applied load of 10 g with a dwell time of 15 s using an NG-1000 CCD microhardness tester. The indentations were made on polished samples within the α-Al matrix. The microhardness value of each condition represented the average of twenty indentations.

3. Results

3.1. As-quenched microstructure

Figure 1 shows the alloy microstructure in the F, PS, and FS conditions. As can be seen in Fig. 1a, the eutectic Si in the F condition was very fine and appeared as a network surrounding the Al matrix due to the rapid solidification of HPVDC. After solutionizing, the Si particles became coarse and separated, as shown in Fig. 1b and c. These features were much more pronounced in the FS condition (Fig. 1c) compared with the PS condition (Fig. 1b) as a result of the increased solution treatment temperature in the former.

The TEM investigation of the as-quenched microstructure revealed the formation of α-Al(MnFe)Si dispersoids during solutionizing in both PS and FS conditions, as shown in Fig. 2a and b, respectively. A $[001]_{\alpha}$ zone axis recorded selected-area electron diffraction pattern (SAEDP) corresponding to Fig. 2a (Fig. 2c) showed faint spots at $\{110\}_{Al}$ positions (arrowed) which characterized these dispersoids [12,13]. The chemical composition of the dispersoids as reported elsewhere [12,14] was also confirmed using TEM-EDS analysis (Fig. 2d). Due to the high Mn content of the alloy (0.53 wt%), α-Al(MnFe)Si dispersoids were precipitated during solutionizing through the decomposition of the highly supersaturated α-Al solid solution produced by the rapid solidification of HPVDC. The size of α-Al(MnFe)Si dispersoids in the FS condition (Fig. 2b) was slightly larger than that in the PS condition (Fig. 2a), which can be attributed to the higher temperature used in the FS condition.

In addition to the α-Al(MnFe)Si dispersoids, scattered precipitates oriented along $<200>_{Al}$ directions were observed in the PS condition, as shown in Fig. 3a. The TEM-EDS analysis of these precipitates (Fig. 3b) showed that they contained Al, Si, and Mg. These precipitates may belong to one of the metastable phases which may possibly be precipitated in between β' and β phases in Al-Mg-Si alloys, including U1, U2, and B′ phases [5,15-18], or the equilibrium β phase. The presence of these precipitates indicates that they were precipitated out of the α-Al solid solution during temperature ramping up to 460 ºC, but they were not fully dissolved back into the α-Al solid solution taking into

consideration the relatively low temperature of 460 ºC in the PS condition. However, such Mg-Si rich precipitates were not detected in the FS condition, which indicates that they were almost completely dissolved into the α-Al solid solution.

3.2. Aged microstructure

The nano-size precipitates formed after aging treatment in the three temper conditions are shown in Fig. 4a-c. For the T5 condition (Fig. 4a), very fine needle-like precipitates were found in the aged microstructure. The length of these precipitates was around 35 nm and they were aligned along $\{200\}_{Al}$ planes. Based on their size and morphology, these precipitates could be defined as fine *β"* precipitates [19-21]. In addition to *β"* precipitates, undefined tiny granular precipitates were also observed spread over the α-Al matrix, which may be precursors of *β"* precipitates. It should be noted that the T5 precipitates of high-pressure die-cast Al-Si-Mg alloys are still debatable and have not yet fully identified in the literature [22,23].

Fig. 4b and c show a quite remarkable evolution occurred in the precipitate microstructure in the T6P and T6F conditions. In the T6P condition (Fig. 4b), the microstructure was dominated by a mixture of fine and relatively large precipitates, which were identified as *β"* and *β'* precipitates based on the SADPs shown in Fig. 4d and e. The *β"* precipitates displayed some streaks along $<100>_{Al}$ directions through $\{200\}_{Al}$ planes (Fig. 4d), whereas *β'* precipitates produced $\{220\}_{Al}$ reflections due to their precipitation on $\{200\}_{Al}$ planes (Fig. 4e). These typical precipitate features were previously described in Refs. [24-26]. Both *β"* and *β'* precipitates were also formed in combination on $\{200\}_{Al}$ habit planes in the T6F condition, as shown in Fig. 4c, but the *β"* precipitates appeared most dominant.

The precipitates formed in the T6P and T6F conditions were compared in terms of their average length and number density, as shown in Fig. 5. The average number density was calculated according to Eq. 1. As can be seen from Fig. 5, the precipitates were denser and smaller in the T6F condition compared to the T6P condition, exhibiting an average length and a number density of, respectively, 88.9 nm and 13202.2 μm^{-3} in the former and 105.5 nm and 4241.4 μm^{-3} in the latter. It is worth mentioning that, taking into consideration their high thermal stability, the α-Al(MnFe)Si dispersoids precipitated during solutionizing were not affected by aging at 185 ºC.

3.3. Evolution of the α-Al solid solution

The evolution of the supersaturation and decomposition of the α-Al solid solution in different conditions was assessed using DSC analysis and both electrical conductivity (EC) and microhardness measurements. Fig. 6 shows the DSC heating curves in the F, FS and PS conditions. The curves exhibited three common exothermic peaks, A, B, and C, at 237-245 ℃, 372-416 ℃, and 462-530 ℃, respectively. These peaks can be attributed to the precipitation of β'', β' and β precipitates, respectively [27]. An endothermic effect (D) occurred in the FS and PS condition that could be related to a partial dissolution of β'' precipitates. Interestingly, the height and area of peaks A, B, and C were remarkably larger in the F condition compared to the FS and PS condition. This indicates that the supersaturation degree of the α-Al solid solution was significantly higher in the F condition due to the rapid solidification of HPVDC, while this degree was generally decreased by conducting solution treatment.

Fig. 7a shows the EC along with the microhardness of the alloy in the F, PS, and FS conditions. Generally, the EC is inversely proportional to the degree of the supersaturation of the α-Al solid solution. The lower the electrical conductivity, the higher is the supersaturation degree, since the solute atoms dissolved in the α-Al matrix could effectively scatter the electrons and consequently decrease the electrical conductivity. As shown in Fig. 7a, the EC exhibited its lowest value of 31.3 %IACS in the F condition, which reveals that the maximum degree of supersaturation was attained in this condition. On the other hand, the EC was increased to 35.9 %IACS and 37.9 %IACS in the FS and PS conditions, respectively, indicating that the supersaturation degree of the α-Al solid solution was decreased in these conditions when compared to the F condition, which is consistent with the DSC results. The microhardness measurements in the F, PS, and FS conditions (Fig. 7a) showed that the F condition had the highest microhardness value followed by the FS and PS conditions (90.0, 87.8 and 82.8 HV, respectively). The microhardness values are given by the extent of the solid solution strengthening which is proportional to the supersaturation degree of the α-Al solid solution. Thus, the results of the DSC, EC and microhardness agree well in the assessment of the supersaturation degree of the α-Al solid solution in the F, PS, and FS conditions.

Fig. 7b shows the EC and microhardness values of the alloy in the T5, T6P, and T6F conditions. The EC increased from 34.3 %IACS in the T5 condition to 40.0 %IACS in the T6P and T6F conditions. The notable difference in the EC values between the T5 condition and both T6P and T6F conditions reveals that the extent of decomposition of the α-Al solid solution after aging at 185 ºC for 4 h was

remarkably varied from the first to the other two conditions. As seen in Fig. 7b, the microhardness varied form one temper to another. The T6F temper yielded the highest microhardness of 107.6 HV, while the T5 and T6P tempers provided lower microhardness values of 100.2 and 96.0 HV, respectively. This indicates that the alloy exhibited different precipitation characteristics after aging in the three temper conditions.

4. Discussion

The TEM observations obviously revealed that the precipitation characteristics of the HPVDC AlSi10Mg0.3Mn alloy differed from the T5 condition to the T6P and T6F conditions. While the precipitation of *β"* phase was still in its early stage in the T5 condition, the precipitation of both *β"* and *β'* phases had already taken place to large extents in the T6P and T6F conditions. Since the alloy was subjected to the same aging treatment (185 ºC for 4 h) in all conditions, the variations in the precipitation characteristics of the alloy are mostly related to the alloy state before aging, namely whether the alloy was as-fabricated or partially or fully solutionized.

The maximum supersaturation degree was achieved in the F condition due to the very high cooling rate and high pressure of the HPVDC, as the solid solubility in this condition is just slightly below the solidus temperature, which would make it possible for the α-Al to retain as much solute atoms as possible. This was confirmed by the highest exothermic peaks (Fig. 6) and the lowest EC in the F condition (Fig. 7a). However, during the T5 aging, the formation of precipitates seemed slow and sluggish, as was confirmed by the TEM results, where *β"* phase was just in its initial stage of precipitation (Fig. 4a). This can be attributed to the relatively low cooling and the subsequent natural aging occurred after ejecting the solidified cast from the die, which would promote the consumption of vacancies and the formation of solute clusters, thereby retarding the precipitation of *β"* phase during artificial aging [28-30]. Therefore, a longer time and/or a higher temperature may be required to reach the peak-aged condition.

For the T6P and T6F tempers, solution treatments and subsequent quenching were involved prior to aging (PS and FS conditions), and therefore abundant quenched-in vacancies were provided in these temper conditions compared with the T5 condition. The precipitation process would, therefore, be faster in the T6P and T6F conditions, resulting in well-developed *β"* and *β'* precipitates (Fig. 4b and c *vs*. Fig. 4a). However, the supersaturation degree of the α-Al in the PS and FS conditions was lower than that in the F condition, which is due to that the solutionizing temperatures in the PS and FS conditions were far

below the solidus temperature and also due to the precipitation of α-Al(MnFe)Si dispersoids in these conditions (Fig. 2). These dispersoids consumed Fe, Mn, and Si solute atoms from the α-Al solid solution, thereby decreasing its degree of supersaturation. This is evidenced by the increases occurred in the EC in the PS and FS conditions compared with the F condition, as shown in Fig. 7a (37.9 and 35.9 %IACS *vs*. 31.3 %IACS). The decreased supersaturation and the consumption of Si solute atoms in the dispersoids explain why the amounts of *β"* and *β'* precipitates, which are mainly composed of Si and Mg, were found to be less in the T6P and T6F conditions compared to the T5 condition using the DSC analysis (Fig. 6, PS and FS *vs*. F). This effect was more pronounced in the PS condition than that in the FS condition. This can be attributed to the presence of Mg-Si rich precipitates that remained undissolved after partial solutionizing (Fig. 3) and consequently further decreased the supersaturation of the α-Al with Si and Mg, whereas they were almost dissolved completely after full solutionizing.

The evolution of the microhardness is related to the microstructure changes in different conditions. In the F, PS and FS conditions, the microhardness is principally given by the solid solution strengthening. As shown in Fig. 7a, the highest microhardness occurred in the F condition (90 HV), which is attributed to the high solid solution strengthening induced by the highest supersaturation of the α-Al in this condition. On the other hand, the reductions of the microhardness appeared in the PS and FS conditions were due to the decreases of the supersaturation level of the α-Al that reduced the solid solution strengthening in these conditions. These reductions seemed to be not fully compensated by the strengthening effect of the α-Al(MnFe)Si dispersoids, since the microhardness displayed lower values in the PS and FS conditions compared to the F condition as shown in Fig. 7a (82.8 and 87.8 HV *vs*. 90.0 HV).

The extent to which the precipitation process took place in the T5, T6F, and T6P conditions would determine the final mechanical properties of the HPVDC AlSi10Mg0.3Mn alloy, which was preliminarily proven by the relevant microhardness values shown in Fig. 7b. Both *β"* and *β'* precipitates were found coexisting in the T6P and T6F conditions, but the *β"* precipitates were much denser and more dominate in the T6F condition, resulting in much higher microhardness in this condition than in the T6P condition (107.6 HV *vs*. 96.0 HV). The *β"* phase has a coherent interface with the α-Al matrix and it is therefore a more effective hardener than the semicoherent *β'* phase [31]. The coherency relationship with the matrix determines the interaction mechanisms between the precipitates of these phases and dislocations and consequently the degree of precipitation hardening. The coherent *β"* precipitates are always sheared by the dislocations, whereas the semicoherent *β'* precipitates are bypassed by the

dislocations [32-34]. A higher applied stress is always necessary for the shearing mechanism compared with the bypassing mechanism to continue moving the dislocations. The hardening produced by the shearing mechanism is due to the chemical strengthening from the energy increase at the additional matrix-precipitate interfaces that form when dislocations shear the coherent precipitates [35,36]. In addition, the interfacial misfit strain induced by the lattice misfit between the coherent precipitates and the matrix contributes to the precipitation hardening through the coherency strengthening [35,37].

In the T5 condition, the alloy was strengthened by both the solid solution strengthening of the residual non-decomposed α-Al solid solution and the *β"* phase that was still in its early stage of precipitation as well as its possible precursors. Because the peak hardening occurs in Al-Mg-Si alloys at the transition from *β"* phase to *β'* phase [38], the alloy did not exhibit its maximum hardness in the T5 condition, displaying a microhardness value lower than that in the T6F condition (100.2 HV *vs*. 107.6 HV), but higher than that in the T6P condition (100.2 HV *vs*. 96.0 HV). Meanwhile, no surface blistering was observed in the T6P and T6F conditions. Therefore, the proposed full solution treatment can further improve the mechanical properties of the HPVDC AlSi10Mg0.3Mn alloy while maintaining casting soundness.

5. Conclusions

1. Both partial and full solution heat treatments of the HPVDC AlSi10Mg0.3Mn alloy resulted in the formation of α-Al(MnFe)Si dispersoids which consumed Fe, Mn, and Si solute atoms from the α-Al solid solution. In addition, Mg-Si rich precipitates formed and remained undissolved after partial solutionizing, causing additional consumptions of Mg and Si solute atoms.
2. The as-fabricated (F) condition achieved the highest supersaturation degree of the α-Al solid solution due to the very high cooling rate and high pressure of the HPVDC process. The supersaturation degree decreased in both partial and full solutionizing conditions.
3. The TEM observations revealed different precipitation characteristics in the T5, T6P and T6F conditions. The precipitation of *β"* phase was still in its early stage in the T5 condition, while the precipitation of both *β"* and *β'* phases had already taken place to different extents in the T6P and T6F conditions.
4. The different precipitation characteristics of the HPVDC AlSi10Mg0.3Mn alloy in the three temper conditions produced different hardening effects that would determine the final alloy mechanical properties. The T6F temper yielded the highest hardening effect followed by the T5

and T6P tempers, providing an approach to improve the mechanical properties of HPVDC parts while avoiding the undesirable surface blistering by optimizing the heat treatment.

Acknowledgments

The authors would like to acknowledge the financial support of the Natural Sciences and Engineering Research Council of Canada (NSERC) under the Grant No. CRDPJ 514651-17 and Rio Tinto Aluminum through the Research Chair in the Metallurgy of Aluminum Transformation at University of Quebec at Chicoutimi.

References

[1] X.P. Niu, B.H. Hu, I. Pinwill, H. Li, Vacuum assisted high pressure die casting of aluminium alloys, Journal of Materials Processing Technology 105 (2000) 119-127.

[2] M. Kohlhepp, P.J. Uggowitzer, M. Hummel, H.W. Höppel, Formation of die soldering and the influence of alloying elements on the intermetallic interface, Materials 14 (2021) 1-16.

[3] S-W Choi, Y-C Kim, C-W Kim, J-I Cho, C-S Kang, Y-M Kim, S-K Hong, Effect of Mn on the interaction between die casting steel and Al alloy, 13th International Conference on Aluminum Alloys (ICAA13), 2012, 225-229.

[4] S. Shivkumar, C. Keller, D. Apelian, Aging behavior in cast Al-Si-Mg alloys, AFS Transactions 98 (1990) 905-911.

[5] R. Vissers, M.A. van Huis, J. Jansen, H.W. Zandbergen, C.D. Marioara, S.J. Andersen, The crystal structure of the β' phase in Al–Mg–Si alloys, Acta Materialia 55 (2007) 3815-3823.

[6] M.A. van Huis, J.H. Chen, M.H.F. Sluiter, H.W. Zandbergen, Phase stability and structural features of matrix-embedded hardening precipitates in Al–Mg–Si alloys in the early stages of evolution, Acta Materialia 55 (2007) 2183-2199.

[7] R.N. Lumley, R.G. O'Donnell, D.R. Gunasegaram, M. Givord, Heat treatment of aluminium alloy high pressure die castings, US Patent US8409374B2 (2013).

[8] J.K. Sunde, Ø. Paulsen, S. Wenner, R. Holmestad, Precipitate statistics in an Al-Mg-Si-Cu alloy from scanning precession electron diffraction data, Journal of Physics: Conference Series 902 (2017) 012022.

[9] S.J. Andersen, Quantification of the Mg_2Si β'' and β' phases in AlMgSi alloys by transmission electron microscopy, Metallurgical and Materials Transactions A 26 (1995) 1931-1937.

[10] S.M. Allen, Foil thickness measurements from convergent-beam diffraction patterns, Philosophical Magazine A 43 (1981) 325-335.

[11] J. Zuo, J. Spence, Electron microdiffraction, Springer Science & Business Media, 2013.

[12] Y.J. Li and L. Arnberg, Quantitative study on the precipitation behavior of dispersoids in DC-cast AA3003 alloy during heating and homogenization, Acta Mater. 51 (2003) 3415–3428.

[13] E.M. Elgallad, K. Liu, Z. Zhang, X.-G. Chen, Effect of transition elements on dispersoid formation and elevated-temperature mechanical properties in 6082 aluminum alloy, Philos. Mag. 101 (2021) 96–116.

[14] K. Liu and X.-G. Chen, Development of Al–Mn–Mg 3004 alloy for applications at elevated temperature via dispersoid strengthening, Mater. Des. 84 (2015) 340–350.

[15] K. Matsuda, Y. Sakaguchi, Y. Miyata, Y. Uetani, T. Sato, A. Kamio, S. Ikeno, Precipitation sequence of various kinds of metastable phases in Al-1.0mass% Mg_2Si-0.4mass% Si alloy, J. Mater. Sci. 35 (2000) 179–189.

[16] S.J. Andersen, C.D. Marioara, R. Vissers, A. Frøseth, H.W. Zandbergen, The structural relation between precipitates in Al–Mg–Si alloys, the Al-matrix and diamond silicon, with emphasis on the trigonal phase U1-$MgAl_2Si_2$, Mater. Sci. Eng. A 444 (2007) 157–169.

[17] W.F. Miao and D.E. Laughlin, Precipitation hardening in aluminum alloy 6022, Scr. Mater. 40 (1999) 873–878.

[18] M. Yang, H. Chen, A. Orekhov, Q. Lu, X. Lan, K. Li, S. Zhang, M. Song, Y. Kong, D. Schryvers, Y. Du, Quantified contribution of β'' and β' precipitates to the strengthening of an aged Al–Mg–Si alloy, Mater. Sci. Eng. A 774 (2020) 138776.

[19] S.J. Andersen, H.W. Zandbergen, J. Jansen, C. Træholt, U. Tundal, O. Reiso, The crystal structure of the β'' phase in Al-Mg-Si alloys, Acta Mater. 46 (1998) 3283–3298.

[20] C.D. Marioara, S.J. Andersen, H.W. Zandbergen, R. Holmestad, The influence of alloy composition on precipitates of the Al-Mg-Si System, Metall. Mater. Trans. A 36 (2005) 691–702.

[21] H. Li, Jy. Wang, Ht. Jiang, Zf. Lü, Zf. Zhu, Characterizations of precipitation behavior of Al-Mg-Si alloys under different heat treatments, China Foundry 15 (2018) 89–96.

[22] E. Yanagihara, S. Orii, T. Iketani, S. Saikawa, K. Matsuda, S. Ikeno, Precipitation structure of Al-10 mass%Si-0.3 mass%Mg alloy produced by high pressure die casting and permanent mold casting with T5 Treatment, Mater. Trans. 56 (2015) 1112–1119.

[23] T. Inoue, M. Goto, A. Yamaguchi, T. Otake, A. Kuroda and M. Yoshida, Effect of pre-aging conditions on T5 heat treatment behavior of Al–9% Si–0.3% Mg die-casting alloy, J. JILM 61 (2011) 507–512.

[24] W. Yang, M. Wang, R. Zhang, Q. Zhang, X. Sheng, The diffraction patterns from *β''* precipitates in 12 orientations in Al–Mg–Si alloy, Scr. Mater. 62 (2010) 705–708.

[25] R.S. Yassar, D.P. Field, H. Weiland, Transmission electron microscopy and differential scanning calorimetry studies on the precipitation sequence in an Al–Mg–Si alloy: AA6022, J. Mater. Res. 20 (2005) 2705–2711.

[26] M.J. Starink and A.-M. Zahra, *β′* and *β* precipitation in an Al-Mg alloy studied by DSC and TEM, Acta Mater. 46 (1998) 3381–3397.

[27] M. Liu, Z. Zhang, F. Breton, X.-G. Chen, Investigation of the quench sensitivity of an AlSi10Mg alloy in permanent mold and high-pressure vacuum die castings, Materials 12 (2019) 1-13.

[28] A. Cuniberti, A. Tolley, M.V. Castro Riglos, R. Giovachini, Influence of natural aging on the precipitation hardening of an AlMgSi alloy, Mater. Sci. Eng. A 527 (2010) 5307-5311.

[29] L. Ding,Y. Weng, S.Wu, R. E. Sanders, Z. Jia, Q. Liu, Influence of interrupted quenching and pre-aging on the bake hardening of Al-Mg-Si alloy, Mater. Sci. Eng. A 651 (2016) 991-998.

[30] M. Mizuno, K. Sugita, H. Araki, Structural transition of vacancy-solute complexes in Al-Mg-Si alloys, Metals 12 (2022) 1-11.

[31] Totten GE, MacKenzie DS. Handbook of Aluminum: Physical metallurgy and processes. New York: Marcel Dekker; 2003.

[32] W.J. Poole, X. Wang, D.J. Lloyd, J.D. Embury, The shearable–non-shearable transition in Al–Mg–Si–Cu precipitation hardening alloys: implications on the distribution of slip, work hardening and fracture, Philos. Mag. 85 (2005) 3113–3135.

[33] K. Teichmann, C.D. Marioara, S.J. Andersen, K. Marthinsen, TEM study of β′ precipitate interaction mechanisms with dislocations and β′ interfaces with the aluminium matrix in Al–Mg–Si alloys, Mater. Charact. 75 (2013) 1–7.

[34] K. Misumi, K. Kaneko, T. Nishiyama, T. Maeda, K. Yamada, K. Ikeda, M. Kikuchi, K. Takata, M. Saga, K. Ushioda, Three-dimensional characterization of interaction between *β"* precipitate and dislocation in Al–Mg–Si alloy, J. Alloys Compd. 43 (2012) 29–33.

[35] H. Fan, A.H.W. Ngan, K. Gan, J.A. El-Awady, Origin of double-peak precipitation hardening in metallic alloys, Int. J. Plast. 111 (2018) 152–167.

[36] M.R. Ahmadi, E. Povoden-Karadeniz, B. Sonderegger, K.I. Öksüz, A. Falahati, E. Kozeschnik, A model for coherency strengthening of large precipitates, Scr. Mater. 84-85 (2014) 47–50.

[37] L.L. Song, S. Liu, X. Mao, A new method for fast statistical measurement of interfacial misfit strain around nano-scale semicoherent particles, RSC Adv. 7 (2017) 28506–28512.

[38] L. Zhen, W.D. Fei, S.B. Kang, H.W. Kim, Precipitation behaviour of Al–Mg–Si alloys with high silicon content, J. Mater. Sci. 32 (1997) 1895–1902.

Figure Captions

Fig. 1. Optical micrographs showing the microstructure in the (a) F, (b) PS, (c) FS conditions.

Fig. 2. (a) and (b) bright-field TEM images showing the α-Al(MnFe)Si dispersoids formed in the PS and FS conditions, respectively, (c) corresponding SAEDP recorded at $[001]_{Al}$ zone axis for (a), and (d) TEM-EDS spectrum showing the composition of the dispersoids.

Fig. 3. (a) bright-field TEM image showing Mg-Si rich precipitates in the PS condition and (b) TEM-EDS spectrum showing the composition of these precipitates.

Fig. 4. (a) to (c) bright-field TEM images showing the precipitates in the T5, T6P and T6F conditions, respectively, and (d) and (e) SAEDPs in the T6P condition.

Fig. 5. Characteristics of the precipitates formed in the T6P and T6F conditions.

Fig. 6. DSC heating curves of the AlSi10Mg0.3Mn alloy in the F, PS and FS conditions.

Fig. 7. EC and microhardness values of the AlSi10Mg0.3Mn alloy in (a) F, PS, and FS conditions, and (b) T5, T6P, and T6F conditions.

Tables

Table 1. Chemical composition (wt%) of the HPVDC alloy.

Si	Mg	Mn	Fe	Ti	Sr	V	Al
10.63	0.32	0.53	0.17	0.05	0.014	0.012	Bal.

Table 2. Tempers applied to the HPVDC AlSi10Mg0.3Mn alloy.

Temper	Solution heat treatment	Aging treatment
T5	N/A*	185°C/4h
T6P	Partial solution treatment, PS: 460°C/1h, followed by water quenching.	185°C/4h
T6F	Full solution treatment, FS: 500°C/1h, followed by water quenching.	185°C/4h

*No solution treatment was applied. The alloy was directly aged in the as-fabricated condition, namely F condition.

Figures

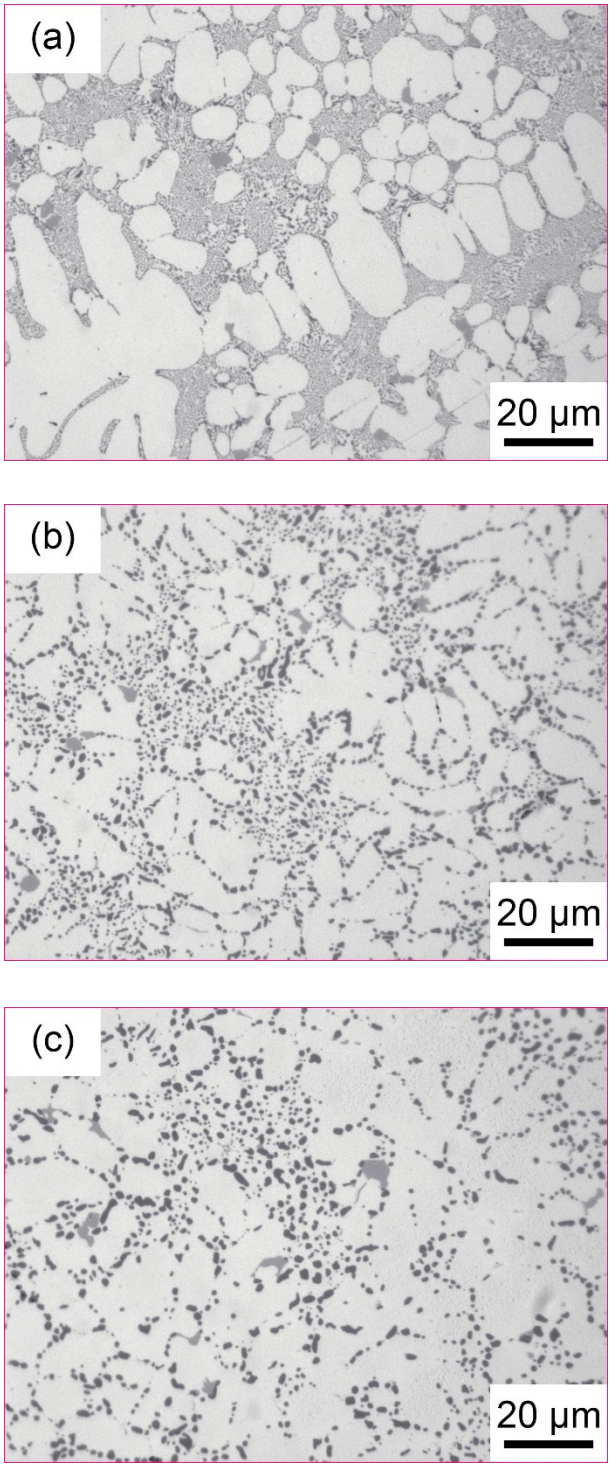

Fig. 1. Optical micrographs showing the microstructure in the (a) F, (b) PS, (c) FS conditions.

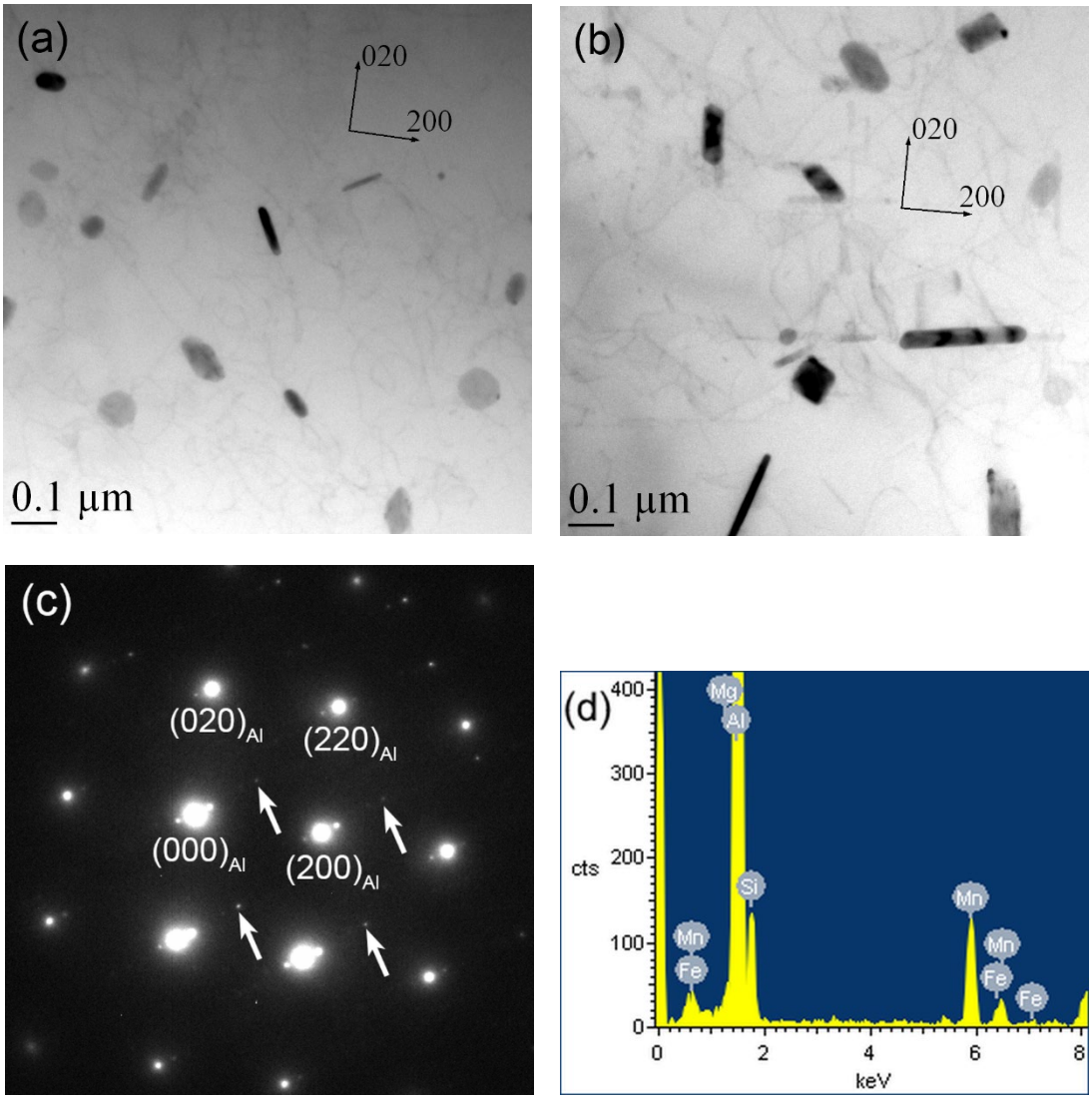

Fig. 2. (a) and (b) bright-field TEM images showing the α-Al(MnFe)Si dispersoids formed in the PS and FS conditions, respectively, (c) corresponding SAEDP recorded at $[001]_{Al}$ zone axis for (a), and (d) TEM-EDS spectrum showing the composition of the dispersoids.

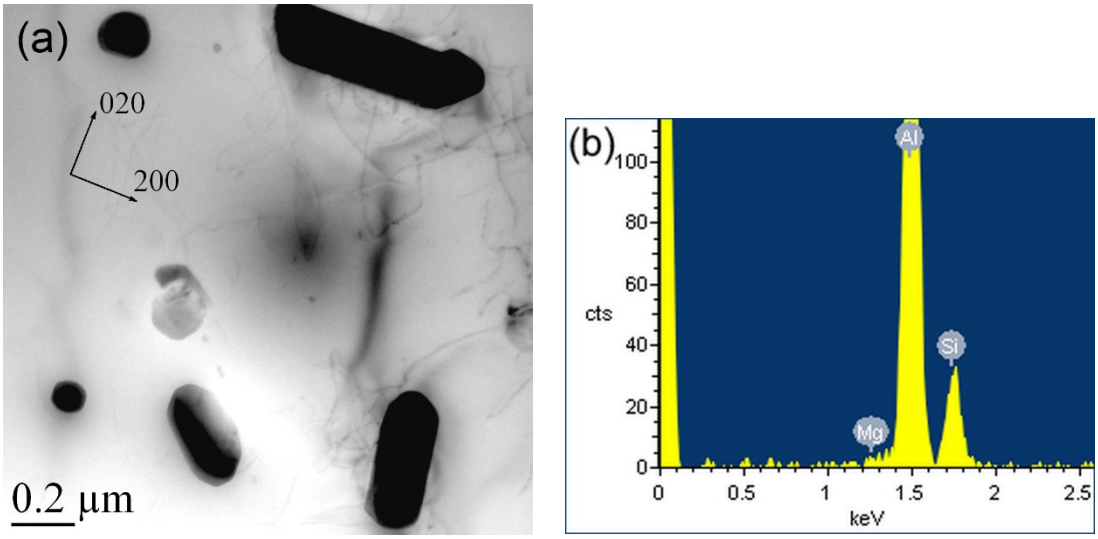

Fig. 3. (a) bright-field TEM image showing Mg-Si rich precipitates in the PS condition and (b) TEM-EDS spectrum showing the composition of these precipitates.

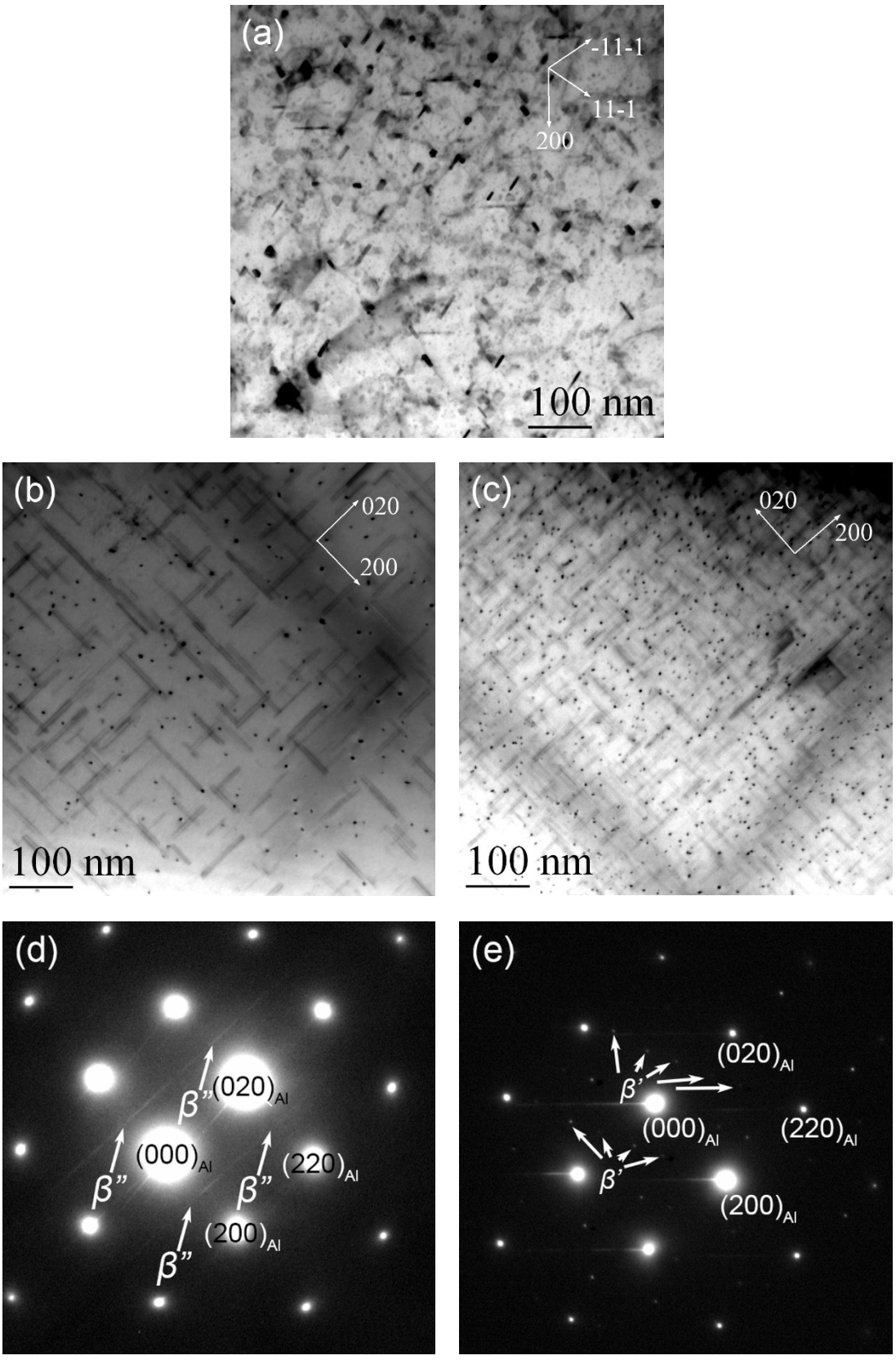

Fig. 4. (a) to (c) bright-field TEM images showing the precipitates in the T5, T6P and T6F conditions, respectively, and (d) and (e) SAEDPs in the T6P condition.

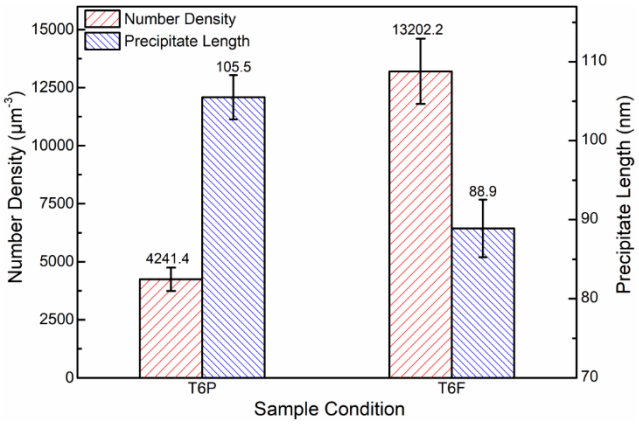

Fig. 5. Characteristics of the precipitates formed in the T6P and T6F conditions.

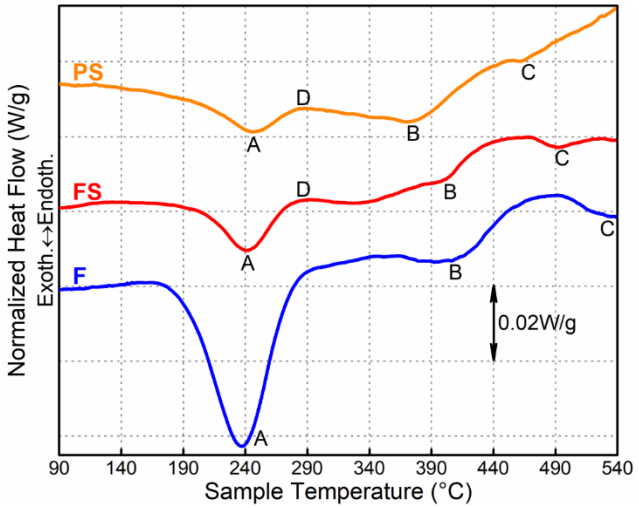

Fig. 6. DSC heating curves of the AlSi10Mg0.3Mn alloy in the F, PS and FS conditions.

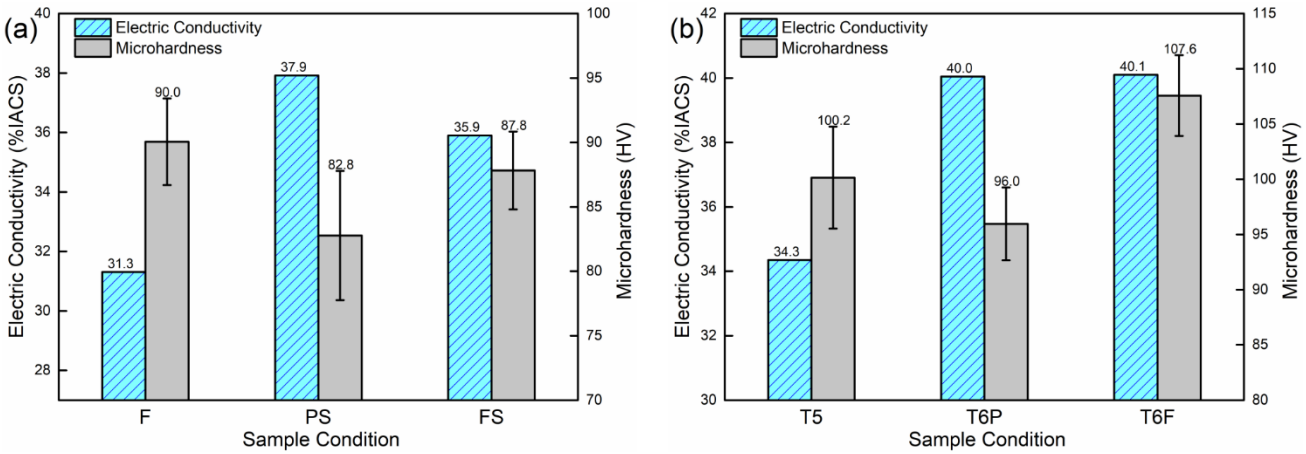

Fig. 7. EC and microhardness values of the AlSi10Mg0.3Mn alloy in (a) F, PS, and FS conditions, and (b) T5, T6P, and T6F conditions.

Supplementary Material

For:

Precipitation Characteristics of HPVDC AlSi10Mg0.3Mn Alloy under Different Temper Conditions

Z. Chen, E.M. Elgallad*, K. Liu, X.-G. Chen

Department of Applied Science, University of Quebec at Chicoutimi,
Saguenay (QC), Canada G7H 2B1

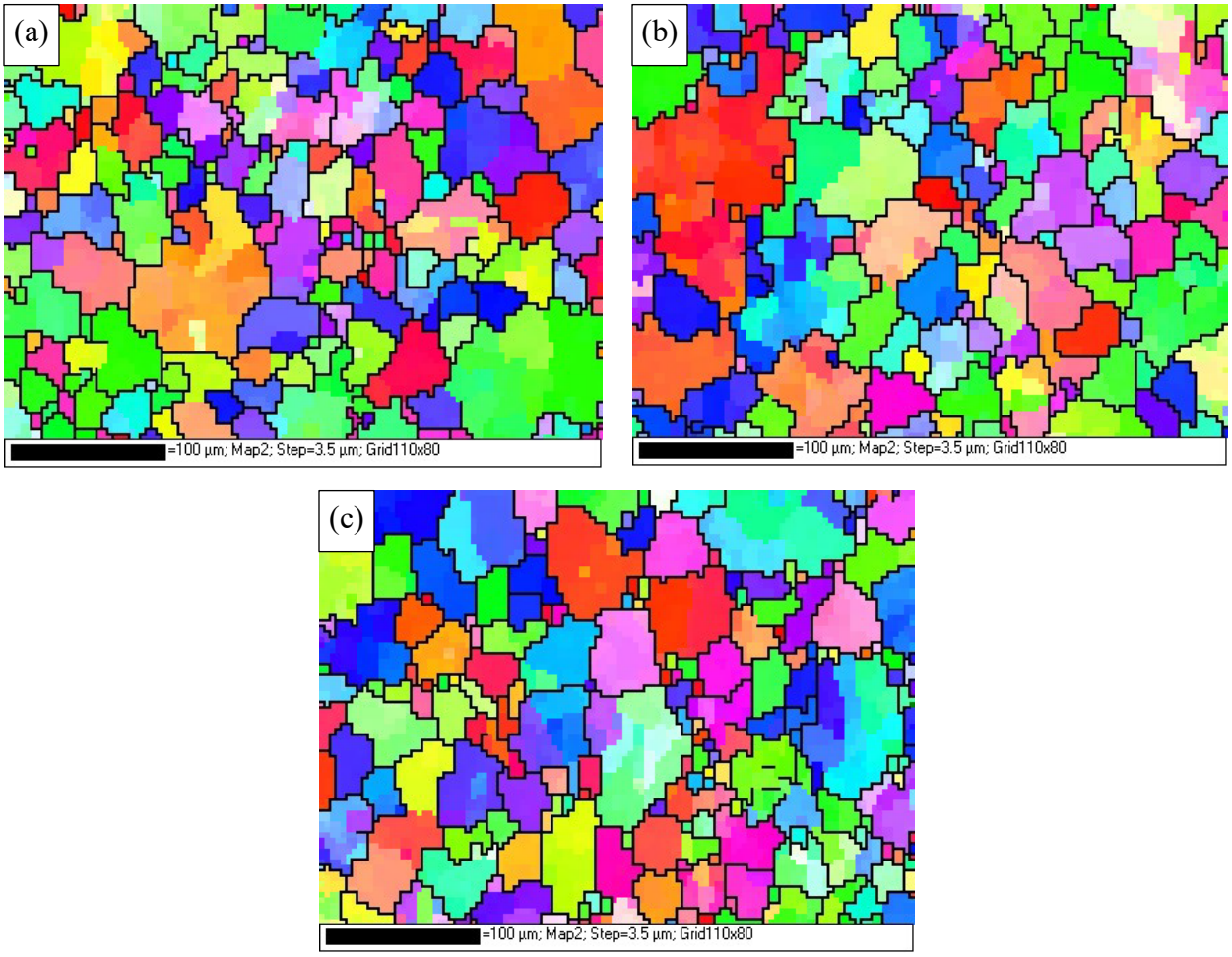

Figure S1. EBSD maps showing the grain structure in: (a) T5, (b) T6P, and (c) T6F temper conditions.

Table S1. Grain size and variation coefficient in the T5, T6P, and T6F conditions based on EBSD analysis.

Condition	Grain size μm			Variation coefficient
	Average	Minimum	Maximum	
T5	25 ± 12	8 ± 4	91 ± 10	0.67
T6P	27 ± 14	9 ± 3	95 ± 12	0.65
T6F	24 ± 14	8 ± 3	89 ± 11	0.68